12 November 2004

CMS NOTE 2004/027

Measurement of the H/A $\rightarrow \tau\tau$ cross section and possible constraints on tanβ

R. Kinnunen[1)], S. Lehti[1)], F. Moortgat[2)], A. Nikitenko[3,a)], M. Spira[4)]

Abstract

The achievable precision of the cross section times branching ratio measurement from the event rates is estimated for the MSSM H/A $\rightarrow \tau\tau$ decay in the associated production process gg $\rightarrow \mathrm{b\bar{b}H/A}$ at large tanβ in CMS. This work demonstrates that the above production and decay process exhibit a large sensitivity to tanβ and thus add as a significant observable to a global fit of the SUSY parameters. To illustrate this potential an example is given concerning the achievable tanβ determination accuracy that could be reached from the event rates and for a given set of SUSY parameters and uncertainties.

[1)] Helsinki Institute of Physics, Helsinki, Finland

[2)] CERN, PH Department, Geneva, Switzerland

[3)] Imperial College, University of London, London, UK

[4)] Paul Scherrer Institut, CH-5232 Villigen PSI, Switzerland

[a)] On leave from ITEP, Moscow, Russia

1 Introduction

The Higgs mechanism is a cornerstone of the Standard Model (SM) and its supersymmetric extensions. Therefore, the search for Higgs bosons is one of the top priorities at future high-energy experiments. Since the Minimal Supersymmetric extension of the Standard Model (MSSM) requires the introduction of two Higgs doublets in order to preserve supersymmetry, there are five elementary Higgs particles, two CP-even (h,H), one CP-odd (A) and two charged ones ($H^{\pm}$). At lowest order all couplings and masses of the MSSM Higgs sector are determined by two independent input parameters, which are generally chosen as tan$\beta = v_2/v_1$, the ratio of the vacuum expectation values of the two Higgs doublets, and the pseudoscalar Higgs boson mass m_A. At leading order (LO) the light scalar Higgs boson mass m_h has to be smaller than the Z boson mass m_Z. Nevertheless the upper bound is significantly enhanced by radiative corrections, the leading part of which grows with the fourth power of the top mass m_t and logarithmically with the stop masses. Therefore, the upper bound on m_h is increased to $m_h \lesssim 135$ GeV/c^2 when one-loop and dominant two-loop corrections are included [1]. The negative direct searches for the Higgsstrahlung processes $e^+e^- \rightarrow Zh/ZH$ and the associated production $e^+e^- \rightarrow Ah/AH$ yield lower bounds of $m_{h,H} > 91.0$ GeV/c^2 and $m_A > 91.9$ GeV/c^2. The range $0.5 <$tan$\beta < 2.4$ in the MSSM is excluded for $m_t = 174.3$ GeV/c^2 by the Higgs searches at the LEP2 experiments [2].

Thus, one of the most important parameters to be determined in the Minimal Supersymmetric Standard Model as well as in a general type-II Two-Higgs Doublet Model (2HDM) is tanβ. In the MSSM tanβ plays a crucial role, since it characterizes the relative fraction of the two Higgs boson doublets contributing to the electroweak symmetry breaking. Consequently, it enters in all sectors of the theory. For small tanβ, it may be possible to determine the value of tanβ within the sfermion or neutralino sector [3, 4]. For large tanβ this method has not been found to be effective. In this regime, however, there are good prospects to measure the value of tanβ by exploiting the Higgs sector [5].

At large tanβ neutral and charged Higgs boson production is dominated by the bremsstrahlung processes $gg \rightarrow b\bar{b}H/A$ and $gb \rightarrow tH^{\pm}$. The dominant parts of the production cross sections are proportional to tan$^2\beta$. For the heavy scalar MSSM Higgs boson H this behavior is valid within 1% for tan$\beta \gtrsim 10$, if the pseudoscalar mass m_A is larger than about 200 GeV/c^2, while for $m_A > 300$ GeV/c^2 it is already satisfied for tan$\beta \gtrsim 5$. Due to this feature the uncertainty on the tanβ measurement is only half of the uncertainty on the rate measurement. In the MSSM the supersymmetric loop corrections introduce an additional tanβ dependence to the cross section [6], but they can be absorbed in an effective parameter tan$\beta_{\rm eff}$, since the dominant terms which are enhanced by tanβ correspond to emission and re-absorption of virtual heavy supersymmetric particles at the bottom Yukawa vertex, which are confined to small space-time regions compared to QCD subprocesses involving massless gluons. The sub-leading terms are small. The dominant terms are universal contributions to the bottom Yukawa coupling [6]. This implies that the method described below determines this effective parameter tan$\beta_{\rm eff}$ in the MSSM (for simplicity, it is denoted everywhere in the rest of the text as tanβ). The extraction of the fundamental tanβ parameter requires additional knowledge of the sbottom and gluino masses as well as the Higgs boson mass parameter μ. These corrections are in general absent in a 2HDM so that in these models the extracted value belongs to the fundamental tanβ parameter. The H/A $\rightarrow \mu\mu$ [7] and H/A $\rightarrow \tau\tau$ decay channels have been identified as the most promising ones for the search of the heavy neutral MSSM Higgs boson H and A at large tanβ. The final states eμ, $\ell\ell$ ($\ell\ell = e\mu, ee, \mu\mu$) [8], lepton+jet [9] and two-jets [10] have been investigated for the H/A $\rightarrow \tau\tau$ decay mode. In this study the m_h^{max} scenario [11] have been chosen with the following MSSM parameters: SU(2) gaugino mass M_2 = 200 GeV/c^2, μ = 300 GeV/c^2, gluino mass $M_{\tilde{g}}$ = 800 GeV/c^2, SUSY breaking mass parameter M_{SUSY} = 1 TeV/c^2 and stop mixing parameter $X_t=\sqrt{6}$ ($X_t=A_t-\mu$cotβ). The top mass is set to 175 GeV/c^2. The Higgs boson decays to SUSY particles are allowed.

In this work the Next-to-Leading Order (NLO) cross section and the branching ratio theoretical uncertainty; and the luminosity and statistical uncertainties are taken into account. The precision on the mass measurement in the H/A$\rightarrow \tau\tau$ channel is estimated and included when trying to determine the precision on the tanβ measurement. The uncertainty on the background as well as the uncertainty on the signal selection efficiency are included as described in Section 4.

The precision that can be achieved in the measurement of the cross section times branching ratio from the event rate within the MSSM for the H/A $\rightarrow \tau\tau$ decay channel in the associated production process $gg \rightarrow b\bar{b}H/A$ at large tanβ is estimated in this study. The work also demonstrates that the above production and decay process exhibits a large sensitivity to tanβ becoming a significant observable to be included in a global fit of the SUSY parameters. To illustrate this potential an example is given concerning the achievable tanβ measurement accuracy that could be reached for the above set of SUSY parameters.

The note is organized as follows: Section 2 describes the event selection and the expected discovery reach. The

measurement uncertainty on the cross section is discussed in Section 3. Section 4 presents the evaluation of the tanβ measurement uncertainty; and in Section 5 the total uncertainty on the tanβ measurement is summarized. Finally, Section 6 is devoted to the conclusions.

2 Event selection and expected discovery reach

This section starts with the comparison between the theoretical NLO cross section and the PYTHIA cross section since PYTHIA has been used for the generation of the hard processes. Then the event selection is discussed, and finally, the expected discovery reach is presented.

2.1 NLO cross section and PYTHIA cross section comparison

Higgs boson production in the $\mathrm{gg} \rightarrow \mathrm{b\bar{b}H/A}$ process was obtained with the PYTHIA [12] two-to-three processes 181 and 186 and with the PYTHIA6.158 default values for the parton distribution functions and the renormalization and factorization scales. No cut on the transverse momentum of the b quarks has been applied at the generation level but $\mathrm{E_T^{jet}} > 20$ GeV is used for the b-jet identification in the event analysis. Therefore it is important to know how well PYTHIA describes the $\mathrm{p_T}$ spectrum of the b quarks compared to the NLO calculations [13] in order to estimate how well the efficiency of the event selection can be determined. The comparison was made for the SM process $\mathrm{gg} \rightarrow \mathrm{b\bar{b}h}$ (PYTHIA process 121) with a Higgs boson mass of 120 GeV/c^2. The PYTHIA and the NLO cross sections are compared in Table 1 as a function of a cut on the transverse momentum of the b quark with highest $\mathrm{p_T}$. In PYTHIA as well as in the NLO calculations the b quark momentum was taken after gluon radiation. The total PYTHIA cross sections ($\mathrm{p_T} > 0$) were normalized to the total NLO cross sections. The agreement between the PYTHIA and the NLO values turns out to be at the level of 5–10%. The statistical uncertainties of the PYTHIA cross sections are shown, too. For completeness the PYTHIA LO cross sections are also compared to the corresponding theoretical LO calculation (the lower two rows in Table 1). In this case the PYTHIA b quark was taken before gluon radiation. Good agreement within 1–2 % has been obtained.

Table 1: Comparison of the NLO and LO cross sections to the PYTHIA cross sections as a function of the cut on the transverse momentum of the b quark with highest $\mathrm{p_T}$. The total PYTHIA cross sections ($\mathrm{p_T} > 0$) are normalized to the corresponding NLO(LO) cross sections.

$\mathrm{p_T}$ cut	0 GeV/c	10 GeV/c	20 GeV/c	30 GeV/c	40 GeV/c	50 GeV/c
σ_{NLO} (pb)	734	507	294	173	106	68
σ_{PYTHIA} (pb)	734	523 ± 3	275 ± 3	156 ± 3	92 ± 2	60 ± 2
σ_{LO} (pb)	528	393	241	152	102	71
σ_{PYTHIA} (pb)	528	407 ± 2	245 ± 3	154 ± 2	101 ± 2	70 ± 2

2.2 Event selection

The event selection for the two-lepton (eμ and $\ell\ell$), lepton+jet (ℓj) and two-jet (jj) final states from H/A/h$\rightarrow \tau\tau$ are described in detail in Refs. [8, 9, 10]. In the region of $\mathrm{M_A} \leq 130$ GeV/c^2 the $\mathrm{gg} \rightarrow \mathrm{b\bar{b}h}$ cross section is comparable to the $\mathrm{gg} \rightarrow \mathrm{b\bar{b}A}$ production cross section, therefore it has been included in the analysis. The relative fractions of these final states are shown in Table 2. The discovery potential in the H/A/h$\rightarrow \tau\tau \rightarrow$ lepton+jet channel is re-evaluated using the cross sections given by the routine HQQ [14] and with updated τ selection and b-tagging efficiencies. Unlike Ref. [9], the recent analysis is extended to large Higgs boson masses, and a 5σ reach up to $\mathrm{m_A} \sim 650$ GeV/c^2 at tan$\beta \sim 50$ is obtained. The details will be described in an upcoming note.

Table 2: Relative fractions of H/A/h$\rightarrow \tau\tau$ final states.

Final state	branching ratio
H/A/h$\rightarrow \tau\tau \rightarrow$ eμ+X	$\sim$6.3%
H/A/h$\rightarrow \tau\tau \rightarrow \ell\ell$+X	$\sim$12.5%
H/A/h$\rightarrow \tau\tau \rightarrow \ell$j+X	$\sim$45.6%
H/A/h$\rightarrow \tau\tau \rightarrow$ jj+X	$\sim$41.5%

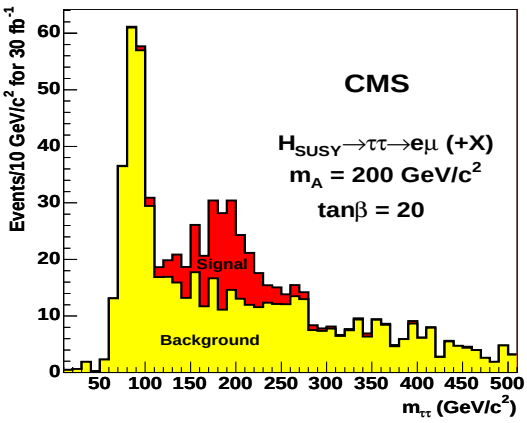

Figure 1: Reconstructed $\tau\tau$ invariant mass in the eμ final state for the H/A/h $\rightarrow \tau\tau$ signal (dark) and for the total background (light) with m_A = 200 GeV/c^2 and tanβ = 20 for 30 fb^{-1}.

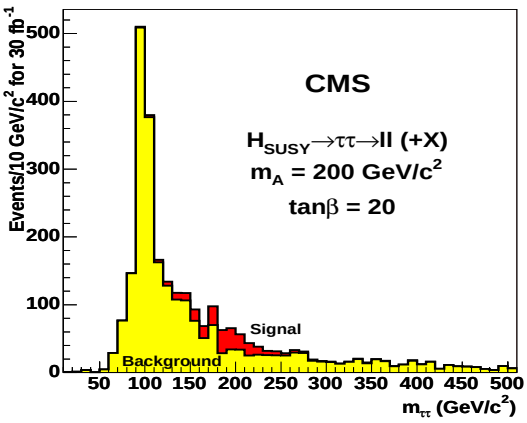

Figure 2: Reconstructed $\tau\tau$ invariant mass in the $\ell\ell$ final state for the H/A/h $\rightarrow \tau\tau$ signal (dark) and for the total background (light) with m_A = 200 GeV/c^2 and tanβ = 20 for 30 fb^{-1}.

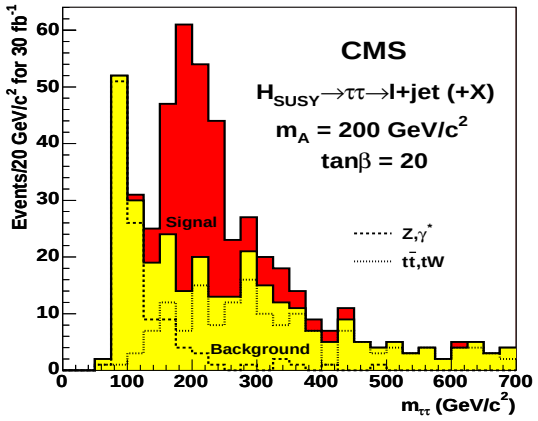

Figure 3: Reconstructed $\tau\tau$ invariant mass in the lepton+jet final state for the H/A/h $\rightarrow \tau\tau$ signal (dark) and for the total background (light) with m_A = 200 GeV/c^2 and tanβ = 20 for 30 fb^{-1}.

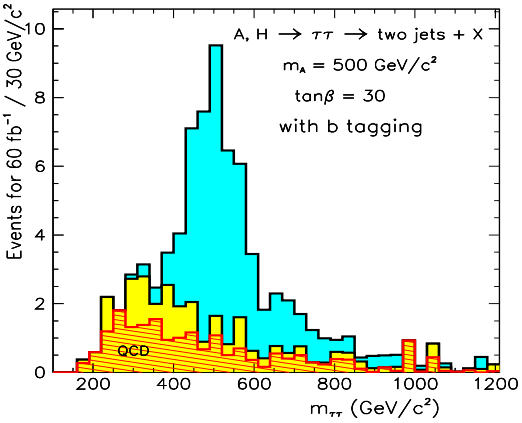

Figure 4: Reconstructed $\tau\tau$ invariant mass for H/A $\rightarrow \tau\tau \rightarrow$ 2 jets (dark), for the total background (light) and for the multi-jet background (dashed) with m_A = 500 GeV/c^2 and tanβ = 30 for 60 fb^{-1}.

The common backgrounds for all the H/A$\rightarrow \tau\tau$ channels are the Z,$\gamma^* \rightarrow \tau\tau$ Drell-Yan process, $t\bar{t}$ production with real and fake τ's and top production Wt. The channels with leptons in the final state suffer from the $b\bar{b}$ background; the W+jet process is the background for the final states with hadronic τ decays. For fully hadronic final states with both τ's decaying hadronically there is in addition the QCD multi-jet background with jets faking τ's, and for the H/A$\rightarrow \tau\tau \rightarrow \ell\ell$+X channel there is the additional background from Z,γ^* decaying to electron and muon pairs.

The hadronic Tau Trigger for the two-jet final state was studied with full simulation in Ref. [10, 15]. For the eμ, $\ell\ell$ and the ℓj final states the trigger was simulated by selecting the kinematic cuts above the trigger thresholds, and taking the trigger efficiencies from Ref. [15]. The used triggers were the Inclusive muon trigger with efficiency 0.9*0.97*0.97 (trigger threshold effect*μ reconstruction efficiency* calorimetric isolation), the Di-electron trigger with efficiency 0.95*0.872*0.946 per electron (trigger threshold effect*Level-1 e efficiency*Level-2 e efficiency) and e-τjet trigger with efficiency 0.95*0.872*0.77*0.95 (e trigger threshold effect*Level-1 e efficiency*HLT e efficiency*τ trigger threshold effect). The backgrounds were suppressed with lepton tracker isolation, τ jet identification, τ tagging with impact parameter, b tagging and jet veto. The τ jet identification [10] selects collimated low multiplicity jets with high p_T charged particles. The hadronic jets are suppressed by a factor of $\sim$ 1000. Tau tagging [8] exploits the short but measurable lifetime of the τ: the decay vertex is displaced from the primary vertex. For b tagging the B hadron lifetime is used to distinguish the associated b jets from c jets and light quark/gluon jets. The Drell-Yan and QCD multi-jet backgrounds are efficiently suppressed with b tagging by a factor of $\sim$ 100,

but it also suppresses the Higgs boson production with no associated b jets. The jet veto is directed against the $\mathrm{t\bar{t}}$ and Wt backgrounds. The rejection of events with more than one jet (including the b jet and not counting τ's) suppresses the $\mathrm{t\bar{t}}$ background by a factor of ~ 5 [10].

Despite several neutrinos in all the H/A$\rightarrow \tau\tau$ final states the Higgs boson mass can be reconstructed. The effective $\tau\tau$ mass was evaluated under the assumption that the neutrinos are emitted along the measured τ decay products. The projection of the missing energy vector onto the neutrinos allowed the neutrino energy estimation. Uncertainties in the missing energy measurement can lead to negative neutrino energies. A significant fraction of the signal events is lost when positive neutrino energies are required, but the backgrounds from $\mathrm{t\bar{t}}$, Wt and QCD multi-jet events are suppressed, since for these backgrounds the neutrinos are generally not emitted along the true or fake τ's. The mass resolution can be improved efficiently with a cut in the $\Delta\phi$ or angular separation between the two τ's. For the two-jet final state in Ref. [10] a mass reconstruction efficiency of 53% has been obtained with the cut $\Delta\phi < 175^o$ and with the requirement of one b jet with $\mathrm{E_T} > 30$ GeV. The reconstructed Higgs boson mass is shown in Figs. 1 to 4 for the four $\tau\tau$ final states. The reconstructed mass peak is a superposition of the H and A signals. In the region $\mathrm{m_A} \lesssim 130$ GeV/c^2 the contribution from the lightest Higgs boson h cannot be separated in these channels and is also included in the signal event rates.

2.3 Expected discovery reach

The 5σ-discovery potential for the H/A/h $\rightarrow \tau\tau$ decay channels with the eμ, $\ell\ell$ and lepton+jet final states for 30 fb^{-1} and with the two-jet final state for 60 fb^{-1} is shown in Figure 5. The 5σ-discovery reach of the H/A $\rightarrow \mu\mu$ decay channel with 60 fb^{-1} is also depicted in the figure. The 5σ-discovery reach obtained after the combination of the eμ, lepton+jet and two-jet final states from the H/A$\rightarrow \tau\tau$ decay channel is shown in Fig. 5 for 30 fb^{-1}. The significance was calculated with the Poisson statistics taking into account the number of signal and background events within the Higgs boson mass window. The combined reach is evaluated by adding the number of signal and background events from the three final states in a given ($\mathrm{m_A}$, tanβ) point. This method, however, can lead to an unsatisfactory result as the analysis of these final states has been optimized to reach the best possible signal significance which has led to different background levels. For example at low values of $\mathrm{m_A}$ and tanβ the signal for the H/A$\rightarrow \tau\tau \rightarrow \ell\ell$+X channel [8] suffers from a significantly larger Drell-Yan background than that for the H/A$\rightarrow \tau\tau \rightarrow$ lepton+jet channel. If the $\ell\ell$ final state is included, the combined reach is smaller than that from the lepton+jet final state alone.

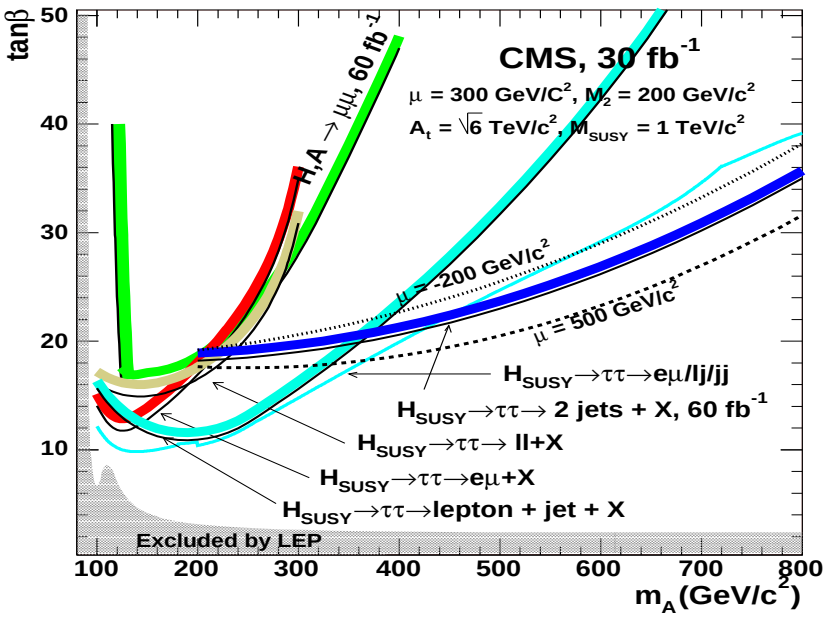

Figure 5: The 5σ-discovery potential for the heavy neutral MSSM Higgs bosons as a function of $\mathrm{m_A}$ and tanβ with maximal stop mixing for 30 fb^{-1}. The H/A $\rightarrow \tau\tau \rightarrow$ two-jet channel is shown for 60 fb^{-1}.

3 Calculation of the cross section measurement uncertainty

The number of signal events after experimental selection is

$$\mathrm{N_S} = \sigma^{\mathrm{prod}} \times \mathrm{L} \times \varepsilon_{\mathrm{sel}}, \tag{1}$$

where σ^{prod} is the cross section times branching ratio, L is the luminosity and $\varepsilon_{\mathrm{sel}}$ is the selection efficiency. The measured value of the cross section times branching ratio is given by

$$\sigma^{\mathrm{prod}} = \sigma_0^{\mathrm{prod}} \pm \Delta\mathrm{stat} \pm \Delta\mathrm{syst}. \tag{2}$$

The considered systematic uncertainties $\Delta\mathrm{syst}$ come from the luminosity, the experimental selection and the background uncertainties. The cross section times branching ratio total uncertainty measurement is the quadratic sum of the statistical and systematic uncertainties:

$$\Delta\sigma^{\mathrm{prod}}/\sigma^{\mathrm{prod}} = \sqrt{\mathrm{N_S} + \mathrm{N_B}}/\mathrm{N_S} \oplus \Delta\mathrm{L}/\mathrm{L} \oplus \Delta\varepsilon_{\mathrm{sel}}/\varepsilon_{\mathrm{sel}} \oplus \Delta\mathrm{N_B^{syst}}/\mathrm{N_S}, \tag{3}$$

where $\mathrm{N_S}$ and $\mathrm{N_B}$ are the number of the signal and background events, $\Delta\mathrm{L}$ is the luminosity uncertainty, $\Delta\varepsilon_{\mathrm{sel}}$ is the experimental selection uncertainty on the signal and $\Delta\mathrm{N_B^{syst}}$ is the background systematic uncertainty.

3.1 Statistical and luminosity errors

The statistical uncertainty from different H/A/h$\rightarrow \tau\tau$ final states are combined using the standard weighted least-squares procedure [16]. The measurements are assumed to be uncorrelated and the weighted error is calculated as

$$\overline{\sigma^{\mathrm{prod}}} \pm \overline{\Delta\mathrm{stat}} = \frac{\Sigma_i w_i \sigma_i^{\mathrm{prod}}}{\Sigma_i w_i} \pm (\Sigma_i w_i)^{-1/2}, \tag{4}$$

where

$$w_i = 1/(\Delta\mathrm{stat}_i)^2. \tag{5}$$

Figure 6 shows the statistical uncertainty on the cross section times branching ratio $\Delta\mathrm{stat}/\sigma^{\mathrm{prod}}$ for the combined eμ + ℓj + jj and $\ell\ell$ + ℓj + jj final states as a function of $\mathrm{m_A}$ for tanβ = 10, 20, 30 and 40, where the signal significance for 30 fb^{-1} exceeds 5σ. The drop in the curves at $\mathrm{m_A}$ = 300 GeV/c^2 is due to fully leptonic final states (eμ and $\ell\ell$) being accessible and included in the tanβ measurement in the region from $\mathrm{m_A}$ = 100 GeV/c^2 to $\mathrm{m_A}$ = 300 GeV/c^2. Similarly, a small decrease is visible at $\mathrm{m_A}$ = 200 GeV/c^2 due to the fully hadronic final state being analyzed only in the region from $\mathrm{m_A}$ = 200 GeV/c^2 to $\mathrm{m_A}$ = 800 GeV/c^2. The statistical uncertainty ranges from 3% to 25% depending on tanβ and $\mathrm{m_A}$.

The uncertainty on the luminosity measurement is assumed to be 5%.

3.2 Uncertainty on the signal selection

The uncertainty on the signal selection efficiency related to the absolute calorimeter energy scale, τ and b-tagging efficiency was taken into account as described in the following.

The calorimeter energy scale introduces an error on the selection efficiency since jets and missing $\mathrm{E_T}$ threshold are required. The full simulation of two tau-jet signal events shows that the assumption of 1 % uncertainty on the calorimeter energy scale [15] leads to $\simeq$ 2.9 % uncertainty on the signal selection efficiency.

The single b-tagging efficiency was evaluated in the following way. Two samples of semileptonic $\mathrm{t\bar{t}}$ events selected for the top quark mass measurement with double b tagging and single b tagging respectively were used. The single b-tagging efficiency is obtained as the ratio of double vs single b-tagged events in the samples, with an additional top mass constraint. Since about 10000 double b-tagged events were obtained after all selections with 30 fb^{-1} [17], the statistical error of the b-tagging efficiency was $\simeq$ 1%. Nevertheless, the b-jet purity and the background

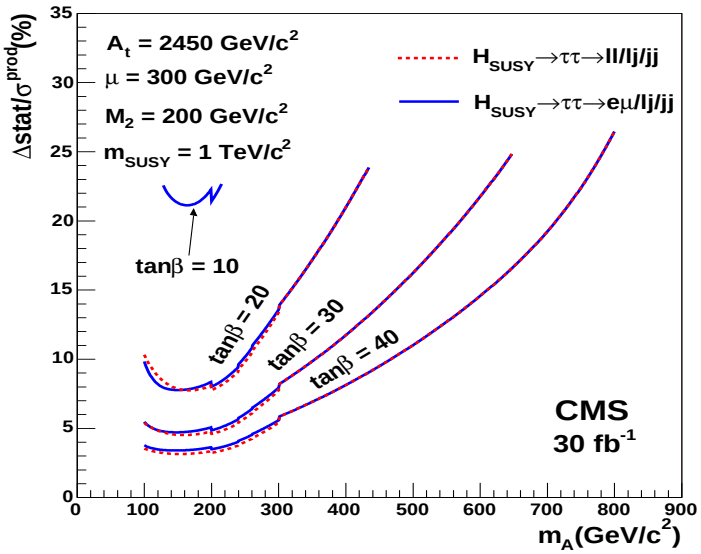

Figure 6: The curves show the statistical uncertainty on the cross section times branching ratio measurement as a function of m_A for tanβ = 10, 20, 30 and 40 where the statistical significance exceeds 5 σ. The uncertainties correspond to 30 fb^{-1}.

contribution for the single b-tagged semileptonic $t\bar{t}$ events still have to be investigated. A value of 2 % for the single b-tagging efficiency uncertainty is taken in this study.

The uncertainty on the τ tagging can be evaluated from the measured ratio of $Z \rightarrow \tau\tau \rightarrow \mu + \tau$ jet and $Z \rightarrow \mu\mu$ events. The background contribution to μ+τ jet final state from $t\bar{t}$ and W+jet events is reduced with the cut on muon plus missing E_T transverse mass , $m(\ell, E_T^{miss})$, and the Z mass constraint. About 10000 $Z \rightarrow \tau\tau \rightarrow \mu + \tau$ jet events are expected with 30 fb^{-1} after muon and τ-jet selections and a cut on $m(\ell, E_T^{miss}) < 30$ GeV/c^2. Thus, the statistical uncertainty on the τ-tagging efficiency is about 1% ($Z \rightarrow \mu\mu$ statistical error is negligible). The cut on $m(\ell, E_T^{miss})$ introduces however about 1 % uncertainty due to the calorimeter energy scale uncertainty. The remaining uncertainty may come from the evaluation of $t\bar{t}$ and W+jet background under the Z mass peak (about 2500 background events are expected before the Z mass constraint with 30 fb^{-1}) and the uncertainty on the muon reconstruction efficiency. Due to these reasons another 2 % was added as a conservative, preliminary estimate leading thus to the total uncertainty on the τ-jet identification efficiency of the order of 2.5 %.

Therefore, the signal experimental selection uncertainty due to the calorimeter energy scale, τ and b-jet tagging efficiency is 4.3 %.

3.3 Background uncertainty

The background uncertainty was evaluated for one representative point of the ($m_A, \tan\beta$) parameter space m_A = 300 GeV/c^2, $\tan\beta$ = 20 and for the H/A$\rightarrow \tau\tau \rightarrow$ lepton+jet channel. The point in the parameter space was chosen close to the 5σ limit where the number of signal events is lowest, and therefore the error $\Delta N_B/N_S$ is largest.

The background after all cuts within a chosen mass window was estimated by fitting the $m_{\tau\tau}$ distribution of the expected background and signal distributions. The error of the fit gives the background uncertainty. The signal mass distribution was approximated with a Gaussian function. The background, however, consists of several different components with different mass distribution shapes. The Drell-Yan background forms a high peak around the Z mass with a long high mass tail. The $t\bar{t}$ and single top backgrounds form a much wider mass distribution. The W+j and $b\bar{b}$ backgrounds were not taken into account in the fit since their contribution to the total background is negligible ($\leq$ 5%).

The shape of the background mass distributions can be obtained from Monte Carlo or directly from the data by relaxing the cuts chosen to suppress the background. The top background can be enhanced by double b tagging (relaxing the central jet veto) which suppresses the signal and Drell-Yan background. The shape of the $t\bar{t}$ background is best fitted with a Landau distribution. The small change of the shape due to the different event selections was

neglected. The Drell-Yan background shape could be evaluated with the suppression of the b tagging requirement. In that case the signal was very small compared to the background. The shape of the Drell-Yan background was also best fitted with a Landau distribution.

Using the shapes for the signal and background distributions, the mass distribution can be fitted varying the number of signal, Drell-Yan and top events. The fit parameters were then used to evaluate the number of background events and its uncertainty in the signal mass window. For the chosen point m_A = 300 GeV/c^2 and $\tan\beta$ = 20 this procedure gives 80.5 signal events and 25.9 background events with ΔN_B = 8.1, which corresponds to a background uncertainty $\Delta N_B/N_S$ = 10%. This uncertainty is used then as a conservative estimate for the whole ($m_A, \tan\beta$) parameter space and for $\ell\ell$ and two τ-jet final states as well.

3.4 Total systematic uncertainty

For the chosen point, m_A = 300 GeV/c^2 and $\tan\beta$ = 20, the total systematic uncertainty is 12 % (the dominat contribution comes from the background uncertainty 10 %) and is of the same order as the statistical uncertainty. The background uncertainty decreases for higher values of $\tan\beta$ at a given value of m_A.

4 Calculation of the tanβ measurement uncertainty

It is clear that the determination of tanβ alone without any knowledge of the other SUSY parameters is not possible, since the branching ratios develop a significant dependence on μ, M_2, A_t and M_{SUSY}. For example, the gaugino sector is sensitive to the values of μ and M_2, and the stop sector and stop mixing is sensitive to the values of μ and A_t. Nevertheless, in order to illustrate the potential of a cross section times branching ratio measurement in the tanβ determination, the SUSY parameters were fixed to the chosen SUSY scenario, but without taking into account the uncertainties, since they are still unknown. Nonetheless, to give an idea of the sensitivity of the signal rate to the SUSY parameters, those were varied by 20 % around the nominal values, as it will be discussed in Section 4.3.

Ignoring in this approach the uncertainties of the other SUSY parameters, the accuracy of the tanβ measurement is due to the uncertainty on the cross section measurement $\Delta\sigma^{prod}$ and the theoretical uncertanty of the cross section calculation.

The branching ratio BR(H/A $\rightarrow \tau\tau$) is approximately constant at large tanβ. At large tanβ the total decay width is dominated by Higgs boson decay to heavy down type fermions, $\tau^+\tau^-$ and $b\bar{b}$ pairs, for which the decay widths have similar tanβ dependence. If the SUSY corrections, which are different for the bottom and τ Yukawa couplings, are not large, the tanβ dependence cancels out in the ratio Γ(H/A $\rightarrow \tau\tau$)/Γ_{tot}, which becomes approximately constant. The counting of signal events measures the total rate $\sigma\times$BR into the chosen final state, which is therefore approximately proportional to tan$^2\beta$. The total rate for the neutral Higgs boson production as a function of tanβ is shown in Fig. 7 for m_A = 300 GeV/c^2.

At large tanβ the production rate can be written as

$$\sigma^{prod} = \tan^2\beta \times X, \tag{6}$$

where X is the tanβ independent part of the production rate. The measured value of tanβ is given by

$$\tan\beta = \tan\beta_0 \pm \frac{1}{2}\Delta\sigma^{prod} \pm \frac{1}{2}\Delta X \tag{7}$$

where ΔX consist of the theoretical uncertainties of the production cross section and the branching ratio, and the uncertainty on the cross section due to the uncertainty on the Higgs boson mass measurement. The total error of $\tan\beta$ is taken as the quadratic sum of $\Delta\sigma^{prod}$ and ΔX:

$$\Delta\tan\beta/\tan\beta = \frac{1}{2}\Delta\sigma^{prod}/\sigma^{prod} \oplus \frac{1}{2}\Delta X/X. \tag{8}$$

4.1 Theoretical uncertainty

The uncertainty on the Next-to-Leading Order cross sections for the gg $\rightarrow b\bar{b}$H/A/h process has been shown to be 20$-$30% for the total rate [13, 18]. It depends, however, on the transverse momentum range of the spectator b quarks and reduces to 10$-$15% with the requirement of $p_T^{b,\bar{b}} \gtrsim$ 20 GeV/c [13, 19, 20]. Therefore, the question about requiring two b jets per event with jet $E_T > 20$ GeV arises naturally. Table 3 shows the number of signal

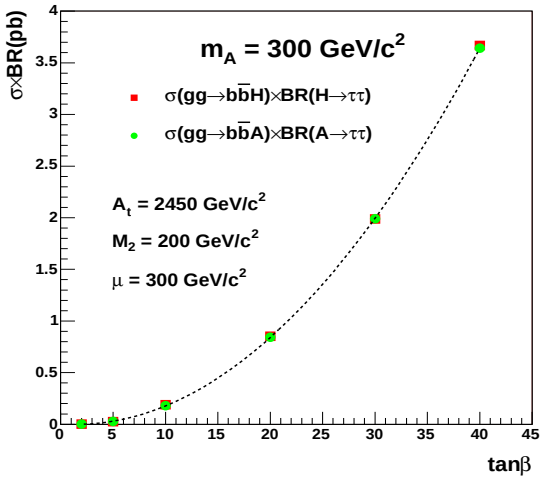

Figure 7: Cross section times branching ratio for $gg \rightarrow b\bar{b}H/A, H/A \rightarrow \tau\tau$ calculated with the programs of Ref. [14].

and background events for the H/A $\rightarrow \tau\tau \rightarrow$ lepton+jet+X channel with m_A = 200 GeV/c^2 and tanβ = 20 for one b-tagged jet in the event (plus a veto on additional jets) and for events with two b-tagged jets. Although the theoretical uncertainty is smaller for events with two b-tagged jets with jet $E_T > 20$ GeV, the decrease of the signal statistics due to low reconstruction and b-tagging efficiency of soft b jets [21] increases the measurement uncertainty. Therefore, only one b jet per event should be tagged in this study. The theoretical uncertainty of about 20% is adopted for the production cross section according to Refs. [13–20]. For the branching ratio the uncertainty is 3% and it is related to the uncertainties of the SM input parameters.

Table 3: The uncertainty on the tanβ measurement for the H/A $\rightarrow \tau\tau \rightarrow$ lepton+jet+X channel for 30 fb^{-1} with one or two b-tagged jets with jet $E_T > 20$ GeV.

m_A = 200 GeV/c^2, tanβ = 20	N_S	N_B	signif.	$\sqrt{N_S + N_B}/N_S$	$\Delta\sigma/\sigma$	$\Delta\tan\beta/\tan\beta^*$
1b-tagging+jet veto	157	70	18.8σ	9.6%	20%	17.3%
2b-tagging	9	44	1.3σ	80.9%	10-15%	48.0-50.5%

*) Statistical + theoretical cross section uncertainties only

4.2 Mass measurement uncertainty

Since the value of the cross section depends on the Higgs boson mass, the uncertainty on the mass measurement leads to an uncertainty on the signal rate. The Higgs mass is measured using the different final states, and the cross section uncertainties due to the mass measurement uncertainty are combined using equations 4 and 5 which give smallest weight to the channels with largest uncertainty. The mass resolution is estimated by fitting the reconstructed $m_{\tau\tau}$ distribution after all selections with a Gaussian function (Fig. 8). The resolution is almost constant as a function of m_A, $\sim$ 24% for the leptonic final state, $\sim$ 17% for the lepton+jet final state and $\sim$ 12% for the hadronic final state as shown in Fig. 9. The fit of the signal plus background distributions (Fig. 10) gives the same Higgs boson mass resolution as the fit of the signal only. The uncertainty on the mass measurement is calculated from the Gaussian fit of the mass peak as $\sigma_{\mathrm{Gauss}}/\sqrt{N_S}$, and the error induced to the cross section ($\Delta\sigma(\Delta m)$) is estimated by varying the cross section for Higgs masses m_0 and $m_0 \pm \sigma_{\mathrm{Gauss}}/\sqrt{N_S}$. At 5$\sigma$ limit where the signal statistics is lowest, the uncertainty on the mass measurement brings 5 - 6% uncertainty on the tanβ measurement.

4.3 Dependence on the SUSY parameters

To give an estimation of the sensitivity of the signal rate to the SUSY parameters, those were varied by 20% around the nominal values. The variation of the signal rate within the expected discovery region is at most $\sim$11% which leads to a maximum of 6% uncertainty on the tanβ measurement. At low m_A the uncertainty is even smaller. As

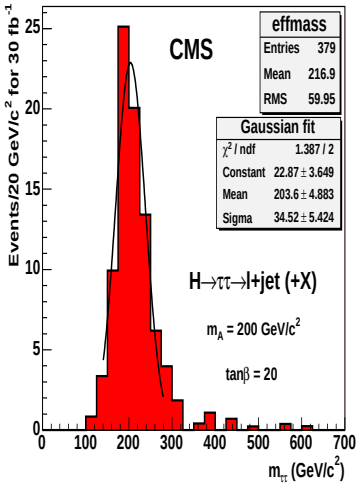

Figure 8: The reconstructed mass of H with Gaussian fit.

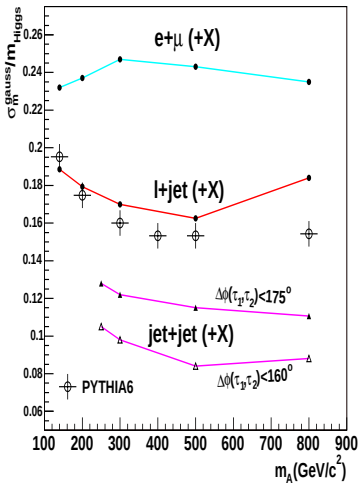

Figure 9: The mass resolution as a function of m_A [8].

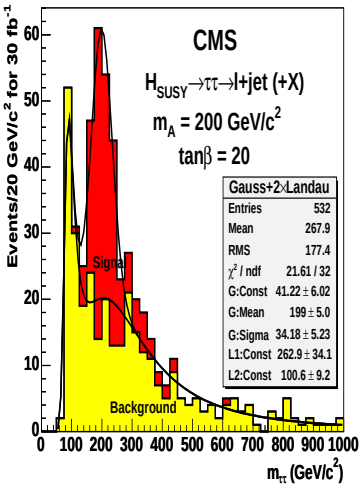

Figure 10: Fit of the signal+background mass distribution.

already stated, in reality, it is expected that the cross section measurement will be entered in a global fit together with the other relevant measurements to determine all SUSY parameters simultaneously.

5 Measurement of tanβ

5.1 H/A $\rightarrow \tau\tau$

Table 4 shows the statistical uncertainty on the tanβ measurement and the uncertainty on the mass measurement for each individual final state and for the combined final states from H/A $\rightarrow \tau\tau$ for 30 fb^{-1}. The total estimated uncertainty is shown for the combined final states. As described in the previous section it includes the following uncertainties: statistical, theoretical, luminosity, mass measurement, uncertainty on the experimental signal selection efficiency and the background uncertainty. The results are shown for the region of the (m_A, tanβ) parameter space where the statistical significance exceeds 5σ. Close to the 5σ limit the statistical uncertainty is of the order of 11 - 12%, but it decreases rapidly for increasing tanβ.

Table 4: Statistical uncertainty on the tanβ measurement and the uncertainties due to the mass measurement for individual and combined final states in four (m_A,tanβ) parameter space points for 30 fb^{-1} with better than 5σ significance. The total uncertainty $\Delta\tan\beta/\tan\beta$ in the Table includes the following uncertainties: statistics, mass measurement, cross section and branching ratio theoretical uncertainties, luminosity, experimental selection efficiency and background uncertainties.

30 fb^{-1}	m_A = 200 GeV/c^2 tanβ = 20		m_A = 200 GeV/c^2 tanβ = 30		m_A = 500 GeV/c^2 tanβ = 30		m_A = 500 GeV/c^2 tanβ = 40	
	Δstat	$\Delta\sigma(\Delta m)$	Δstat	$\Delta\sigma(\Delta m)$	Δstat	$\Delta\sigma(\Delta m)$	Δstat	$\Delta\sigma(\Delta m)$
H/A$\rightarrow \tau\tau \rightarrow e\mu$	8.95%	4.82%	4.85%	3.27%	-	-	-	-
H/A$\rightarrow \tau\tau \rightarrow \ell\ell$	7.96%	3.50%	4.08%	2.37%	-	-	-	-
H/A$\rightarrow \tau\tau \rightarrow \ell$j	4.81%	2.46%	2.84%	1.65%	-	-	8.40%	4.82%
H/A$\rightarrow \tau\tau \rightarrow$jj	13.7%	4.73%	8.25%	3.21%	12.4%	5.82%	8.45%	4.44%
Combined	4.05%	1.99%	2.35%	1.34%	9.09%	4.28%	5.96%	3.26%
eμ+ℓj+jj	$\Delta\tan\beta/\tan\beta$		$\Delta\tan\beta/\tan\beta$		$\Delta\tan\beta/\tan\beta$		$\Delta\tan\beta/\tan\beta$	
	12.59%		12.06%		15.46%		13.57%	
Combined	3.94%	1.85%	2.24%	1.25%	9.09%	4.28%	5.96%	3.26%
$\ell\ell$+ℓj+jj	$\Delta\tan\beta/\tan\beta$		$\Delta\tan\beta/\tan\beta$		$\Delta\tan\beta/\tan\beta$		$\Delta\tan\beta/\tan\beta$	
	12.53%		12.03%		15.46%		13.57%	

As shown in the table, the highest statistical accuracy of about 5% for m_A = 200 GeV/c^2 and tanβ = 20, is

obtained with the lepton+jet final state. Combining other channels with the lepton+jet channel in this mass range improves the precision only slightly. The difference between the fully leptonic channels (eμ and $\ell\ell$) is small: the statistical uncertainty is slightly smaller for the eμ channel, if m_A is close to the Z peak, but already at m_A = 200 GeV/c^2 the final state with any two leptons yields better statistics and lower uncertainties. The combined $\ell\ell$+ℓj+jj channel yields a slightly smaller statistical error at tanβ = 20 than the combined eμ+ℓj+jj channel despite the larger backgrounds in the $\ell\ell$ final state.

Figure 11 shows the statistical uncertainty and the statistical plus systematic uncertainties on tanβ for the combined eμ + ℓj + jj and $\ell\ell$ + ℓj + jj final states as a function of m_A for tanβ = 20, 30 and 40, and for 30 fb^{-1}. The total uncertainty ranges from 12% to 19% depending on tanβ and M_A.

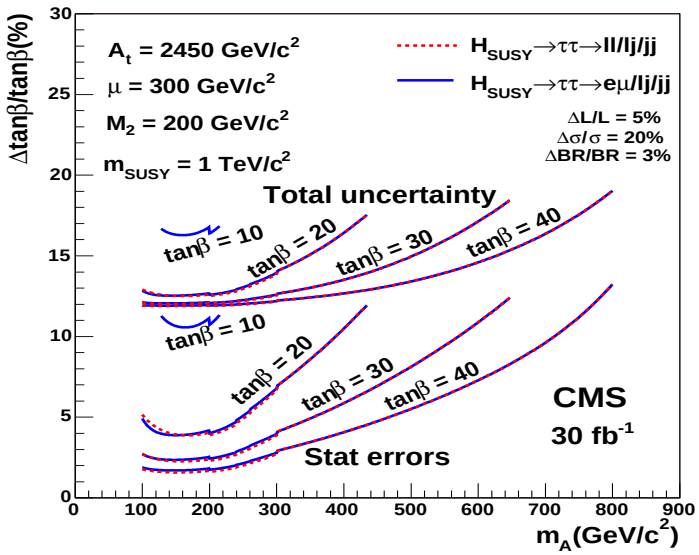

Figure 11: Measurement uncertainty on tanβ: the three lower curves show the uncertainty on tanβ measurement when only the statistical uncertainty is taken into account. The three upper curves show the total uncertainty evaluated as described in the text. The uncertainty correspond to 30 fb^{-1}.

Figures 12 and 13 show the uncertainty on the tanβ measurement with error bars for the combined eμ + ℓj + jj channel for 30 and 60 fb^{-1} at low luminosity. The statistical uncertainties are depicted by the smaller error bars and gray area, the uncertainties including the systematic errors are presented with longer error bars. The errors are shown in the region with signal significance larger than 5σ. The combined 5σ reach is plotted with the contribution from the eμ final state included up to m_A = 180 GeV/c^2 in order to extend the reach to lower tanβ values. For the same reason at very high values of m_A only the two-jet final state contributes to the reach. The errors are calculated within the shown 5σ reach using all available information, including leptonic final states for $m_A < 300$ GeV/c^2, and ℓj final state for $m_A < 800$ GeV/c^2. The statistical uncertainty is largest close to the 5σ limit, where the combination of the different final states improves the accuracy.

5.2 H/A $\rightarrow \mu\mu$

In the region $m_A \lesssim 300$ GeV/c^2, the value of tanβ could also be measured in the H/A$\rightarrow \mu\mu$ channel using event rates. In this channel, the Higgs mass resolution is about 2% [7]. Therefore the total width of the Higgs boson could be measured with good precision from the Higgs boson mass peak. The variation of the natural width as a function of tanβ, from less than 1 GeV/c^2 to about 20 GeV/c^2 in the expected tanβ range, could be used to determine the value of tanβ. This method, based on the direct width measurement, would therefore be complementary to the method explained in this note.

6 Conclusion

The precision of the cross section times branching ratio, $\sigma^{\rm prod}$, measurement and the derived tanβ value was estimated in the H/A $\rightarrow \tau\tau$ decay channel with two-lepton, lepton+jet and two-jet final states for 30 fb^{-1}. The

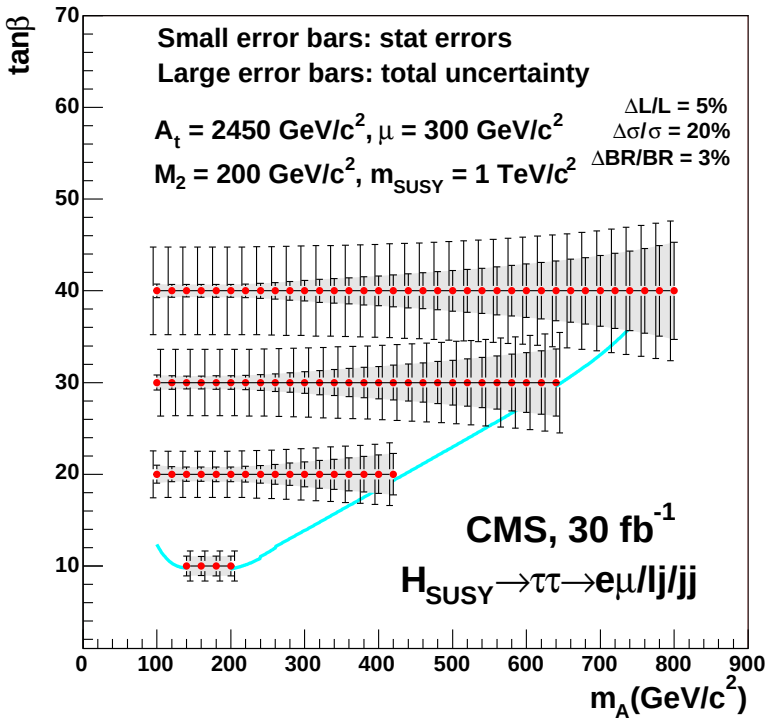

Figure 12: The uncertainty on the tanβ measurement shown as error bars. The small error bars and gray area show the statistical errors only. The large error bars show the total uncertainty evaluated as described in the text. The solid curve corresponds to the 5σ-discovery contour of Fig. 5. Those results correspond to 30 fb^{-1} of integrated luminosity.

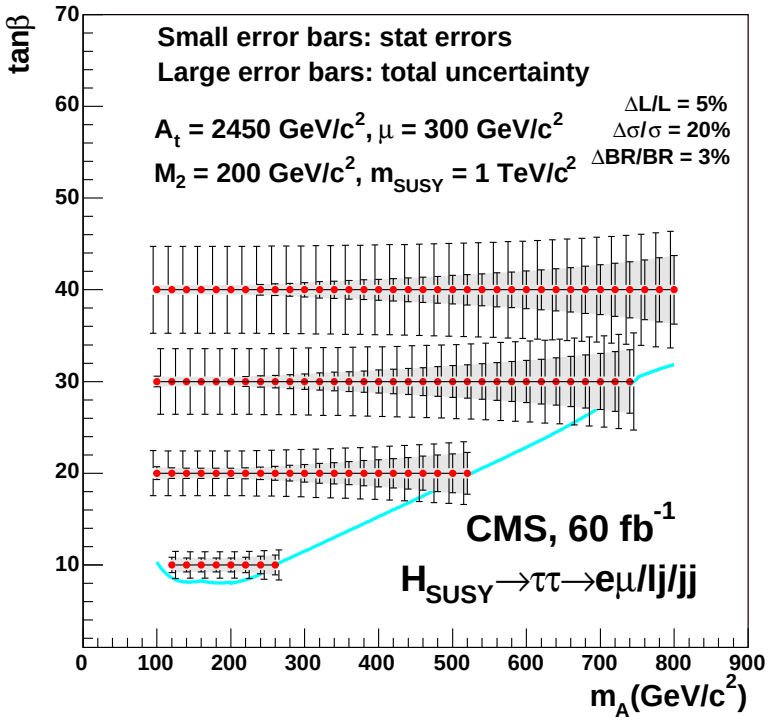

Figure 13: The same as in Fig. 12 but with 60 fb^{-1} taken at low luminosity.

statistical precision on $\sigma^{\rm prod}$ is expected to be $3-25$ % and the associated systematic error ≤ 12 % both depending on the signal significance.

In the region of large tanβ, the tan$^2\beta$ dependence of the associated production processes $\rm gg \rightarrow b\overline{b}H/A$ has been exploited to obtain a statistical uncertainty being a factor of two smaller than that of the event rates. Due to the presence of potentially large radiative corrections to the bottom Yukawa coupling, the results obtained in this analysis correspond to an effective parameter tanβ_{eff} which absorbs the leading universal part of these corrections. A theoretical error of 20% (cross section) and 3% (branching ratio) and a luminosity uncertainty of 5% have been assumed. If two b jets with $\rm E_T > 20$ GeV are tagged, the theoretical uncertainty on the cross section reduces to 10-15%, but the event rates have been found to decrease significantly leading to a worse accuracy of the tanβ measurement. With one tagged b jet in the event the total uncertainty on tanβ estimated with the H/A $\rightarrow \tau\tau$ decay channels ranges from 12% to 19% within the 5σ-discovery reach depending on tanβ and $\rm M_A$ after collecting 30 fb^{-1}. The combination of the $\rm e\mu$, ℓ+jet and two-jet or $\ell\ell$, ℓ+jet and two-jet final states gives 4% better statistical accuracy than the best individual final state. Close to the 5σ-discovery limit the statistical uncertainty ranges in the same order as the theoretical one, but for tanβ regions where the signal significance exceeds 5σ significantly the theoretical error dominates.

7 Acknowledgments

The authors would like to thank Michael Krämer, Fabio Maltoni, Tilman Plehn, Torbjörn Sjöstrand, Georg Weiglein and Scott Willenbrock for helpful comments and discussions.

The authors would like to thank the members of the CMS Editorial Board Reyes Alemany Fernandez and Luc Pape for many useful comments which improved the paper.

References

[1] M. Carena and H.E. Haber, hep-ph/0208209 and references therein.

[2] LEP Higgs Working Group for Higgs boson searches, Proceedings International Europhysics Conference on High Energy Physics (HEP 2001), Budapest, Hungary, 12-18 Jul 2001, hep-ex/0107029 and hep-ex/0107030.

[3] H. Baer, C. Chen, M. Drees, F. Paige, X. Tata, Phys. Rev. **D 59** (1999) 055014.

[4] D. Denegri, W. Majerotto and L. Rurua, Phys. Rev **D 60** (1999) 035008.

[5] J.F. Gunion, L. Poggioli, R. Van Kooten, C. Kao and P. Rowson, hep-ph/9703330.

[6] L. J. Hall, R. Rattazzi and U. Sarid, Phys. Rev. **D 50** (1994) 7048; M. Carena, M. Olechowski, S. Pokorski and C. E. Wagner, Nucl. Phys. **B 426** (1994) 269; M. Carena, D. Garcia, U. Nierste and C. E. Wagner, Nucl Phys. **B 577** (2000) 88; J. Guasch, P. Häfliger and M. Spira, hep-ph/0305101.

[7] R. Kinunnen and I.K. Furic, CMS Note 1998/039; L. Bellucci, MSSM Neutral Higgs Boson searches at CMS in the $\mu\mu$ channel, Dissertation, Universita degli studi di Firenze, December, 2001.

[8] S. Lehti, Prospects for the Detection of the MSSM Higgs Bosons Decaying into Tau Leptons in the CMS Detector, Dissertation, University of Helsinki, Report Series in Physics, HU-P-D93, 2001.
S. Lehti, CMS NOTE 2002/035.

[9] R. Kinnunen and A. Nikitenko, CMS NOTE 1997/106.

[10] R. Kinnunen and A. Nikitenko, CMS NOTE 2003/006.

[11] M. Carena, S. Heynemeyer, C.E.M. Wagner and G. Weiglein, hep-ph/0202167.

[12] T. Sjöstrand, P. Eden, Ch. Friberg, L. Lönnblad, C. Miu, S. Mrenna and E. Norrbin, Comput. Phys. Commun. **135** (2001) 238.

[13] S. Dittmaier, M. Spira and M. Krämer, hep-ph/0309204.

[14] M. Spira, Fortschr. Phys. 46 (1998) 203.

[15] CERN/LHCC 2002-26, CMS TDR 6.2.

[16] K. Hagiwara *et. al.*, Phys. Rev. **D 66** (2002) 010001.

[17] L. Sonnenschein, CMS NOTE 2001/001.

[18] T. Plehn, Phys. Rev. **D67** (2003) 014018, hep-ph/0206121; E. Boos and T. Plehn, hep-ph/0304034.

[19] J. Campbell *et. al.*, hep-ph/0204093.

[20] S. Dawson, C.B. Jackson, L. Reina and D. Wackeroth, hep-ph/0311067.

[21] S. Lehti, CMS NOTE 2001/019.